

TWO-DIMENSIONAL SOLITONS IN IRREGULAR LATTICE SYSTEMS

M. J. Ablowitz,^{*} B. Ilan,[†] E. Schonbrun,[‡] and R. Piestun[‡]

We compute and study localized nonlinear modes (solitons) in the semi-infinite gap of the focusing two-dimensional nonlinear Schrödinger (NLS) equation with various irregular lattice-type potentials. The potentials are characterized by large variations from periodicity, such as vacancy defects, edge dislocations, and a quasicrystal structure. We use a spectral fixed-point computational scheme to obtain the solitons. The eigenvalue dependence of the soliton power indicates parameter regions of self-focusing instability; we compare these results with direct numerical simulations of the NLS equation. We show that in the general case, solitons on local lattice maximums collapse. Furthermore, we show that the N th-order quasicrystal solitons approach Bessel solitons in the large- N limit.

Keywords: soliton, localized lattice mode, nonlinear optics, beam self-focusing, quasicrystal

1. Introduction

Solitons are localized nonlinear waves and occur in many branches of physics. Their properties have provided a deep and fundamental understanding of complex nonlinear systems. In recent years, there has been considerable interest in studying solitons in systems with periodic potentials or lattices, in particular, those that can be generated in nonlinear optical materials [1]–[5]. In periodic lattices, solitons can form when their propagation constant, or eigenvalue, is within certain regions, often called gaps, a concept that is borrowed from the Floquet–Bloch theory for linear propagation. But the external potential of complex systems can be much more general and physically richer than a periodic lattice. For example, atomic crystals can have various irregularities, such as defects and edge dislocations, and also quasicrystal structures, which have long-range orientational order but no translational symmetry [6]–[8]. In general, when the lattice periodicity is slightly perturbed, the band–gap structure and soliton properties also become slightly perturbed, but solitons are otherwise expected to exist in much the same way as in the perfectly periodic case [9], [10]. But the existence and properties of multidimensional solitons when the external potential has *large variations from periodicity* has remained largely unexplored.

In this study, we find two-dimensional (2D) solitons in lattices that have vacancy defects, edge dislocations, and quasicrystal structures. We use a fixed-point spectral method to compute the ground states of the underlying nonlinear Schrödinger (NLS) equation. We find solitons on irregular lattices similarly to solitons on periodic lattices. A comparative study of the eigenvalue dependence of the soliton power leads to important observations regarding soliton power, gap edge, and stability properties. We investigate the evolution by direct numerical simulation, showing that slightly perturbed solitary waves in irregular

^{*}Department of Applied Mathematics, University of Colorado, Boulder, Colo. 80309-0526, USA.

[†]School of Natural Sciences, University of California, Merced, P.O. Box 2039, Merced, Calif. 95344, USA, e-mail: bilan@ucmerced.edu.

[‡]Department of Electrical and Computer Engineering, University of Colorado, Boulder, Colo. 80309-0425, USA.

lattices can either oscillate with small or large amplitudes or collapse. We note that the physical properties of optically generated quasicrystal potentials have generated significant interest and localized defects in optical lattices have recently been constructed [11], [12]. Our results can also be applied to photonic band-gap systems, for which novel experimental techniques have recently been used to fabricate irregular lattice structures [12]–[15].

We study the nonlinear system governed by the focusing (2+1)-dimensional NLS equation (in dimensionless units) with an external potential,

$$iu_z + \Delta u + |u|^2 u - V(x, y)u = 0. \quad (1)$$

In optics, $u(x, y, z)$ corresponds to a complex-valued slowly varying amplitude of the electric field in the xy plane propagating in the z direction (which also plays the role of time), $\Delta u \equiv u_{xx} + u_{yy}$ corresponds to diffraction, the cubic term in (1) originates from the nonlinear (Kerr) change in the refractive index, and the potential $V(x, y)$ corresponds to a modulation of the linear refractive index of the medium. Equation (1) also governs the dynamics of certain Bose–Einstein condensates (BECs), where $u(x, y, z)$ represents the wave function of the mean-field atomic condensate that is trapped in a potential [16].

We seek localized solutions of Eq. (1) in the form $u(x, y, z) = f(x, y)e^{-i\mu z}$, where μ is the propagation constant (or eigenvalue) and $f(x, y)$ is a real-valued localized function that, in accordance with Eq. (1), satisfies the nonlinear eigenequation

$$\Delta f + [\mu + |f|^2 - V(x, y)]f = 0. \quad (2)$$

In this study, we consider potentials that can be written as the intensity of a sum of N phase-modulated plane waves, i.e.,

$$V(x, y) = \frac{V_0}{N^2} \left| \sum_{n=0}^{N-1} e^{i\vec{k}_n \cdot \vec{x} + i\theta_n(x, y)} \right|^2, \quad (3)$$

where $V_0 > 0$ is constant, $\vec{x} = (x, y)$, \vec{k}_n is a wave vector, $\theta_n(x, y)$ is a phase function that introduces irregularities, and normalizing by N^2 means that V_0 is the peak depth of the potential, i.e., $V_0 = \max_{x, y} V(x, y)$. Such 2D potentials can be physically realized in optics by the interference of plane waves and phase functions [12]. For example, these phase functions can be composed of different vortex configurations [17], which can in turn be created using computer-generated holograms [12].

We compute soliton solutions of Eq. (2) using a fixed-point spectral computational method [18] (see the appendix).

2. Band-gap structure

It is well known that if Eq. (2) were linear and the potential were periodic, i.e.,

$$\Delta f + [\mu - V(\vec{x})]f = 0, \quad V(\vec{x}) = V(\vec{x} + \vec{L}),$$

then Floquet–Bloch theory guarantees that the solution could be written as

$$f(\vec{x}) = e^{i\vec{k} \cdot \vec{x}} p(\vec{x}),$$

where $p(\vec{x}) = p(\vec{x} + \vec{L})$ is a bounded function with the same periodicity as $V(x, y)$ and $\vec{k}(\mu) = (k_1, k_2)$ can belong to one of the following three categories (cf. [19]):

- $\vec{k}(\mu)$ is real valued, in which case $f(\vec{x})$ is bounded and μ is said to be in a band (or spectrum);

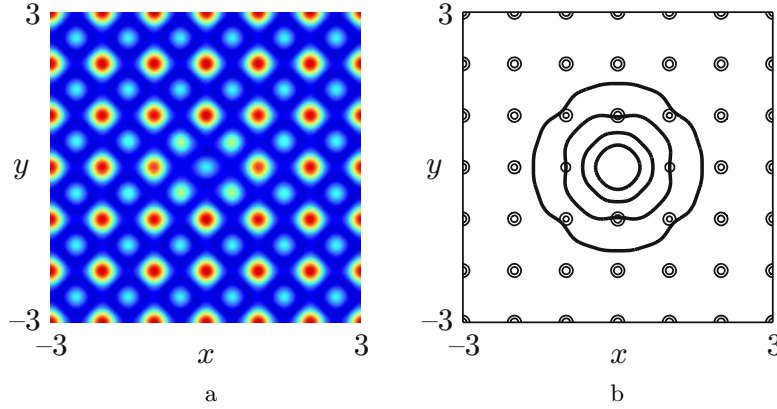


Fig. 1. (a) Contour image of a lattice with a vacancy defect, i.e., the potential in (4) with $V_0 = 12.5$ and $K = k_x = k_y = 2\pi$. The dark spots correspond to local maximums. (b) Contour plot of the soliton with $\mu = 0.5$ superimposed on the lattice. For visibility, only a small portion of the $[-10, 10]^2$ computational domain is presented.

- $\vec{k}(\mu)$ is strictly complex, $f(\vec{x})$ is unbounded, and μ is in a gap; or
- $e^{i\vec{k}\cdot\vec{L}} = \pm 1$, $f(\vec{x})$ is (quasi)periodic, which occurs in the general case for a countably infinite sequence of eigenvalues $\mu_1 < \mu_2 < \dots$ with the limit point at infinity.

In this study, we are interested in *localized nonlinear*, not linear, states. Moreover, the potential is not periodic. Nevertheless, the band-gap notion is still useful in these cases. We compute nonlinear localized states in the semi-infinite gap $-\infty < \mu < \mu_{\max}$, where μ_{\max} is the gap edge, equal to the maximum value for which the computational method converges to the localized mode.

3. Vacancy defect

The first type of potential (3) that we study is an irregular 2D square lattice with a *vacancy defect* (see Fig. 1a),

$$V(x, y) = \frac{V_0}{25} |2 \cos(k_x x) + 2 \cos(k_y y) + e^{i\theta(x, y)}|^2 \quad (4)$$

with $k_x = k_y = K$, where the phase function $\theta(x, y)$ is given by

$$\theta(x, y) = \arctan\left(\frac{y - y_0}{x}\right) - \arctan\left(\frac{y + y_0}{x}\right).$$

Physically, $\theta(x, y)$ corresponds to two first-order phase dislocations displaced by the distance $2y_0$ in the y direction. A vacancy defect can thus be obtained using $y_0 = \pi/K$. We note that the “vacancy” at the origin is created from a continuous function and that potential (4) far from the origin is locally a square lattice with the period $2\pi/K$. Using the computational method described in the appendix, we find localized modes (solitons) of Eq. (2) with potential (4) with a center near the vacancy, as shown in Fig. 1b. In certain respects, they resemble solitons with a center near a minimum of a periodic square lattice. In further investigations, we find that if the soliton center is moved farther from the vacancy, then its profile and band-gap structure converge to those of the corresponding periodic lattice (i.e., we obtain Eq. (4) with $\theta(x, y) \equiv 0$).

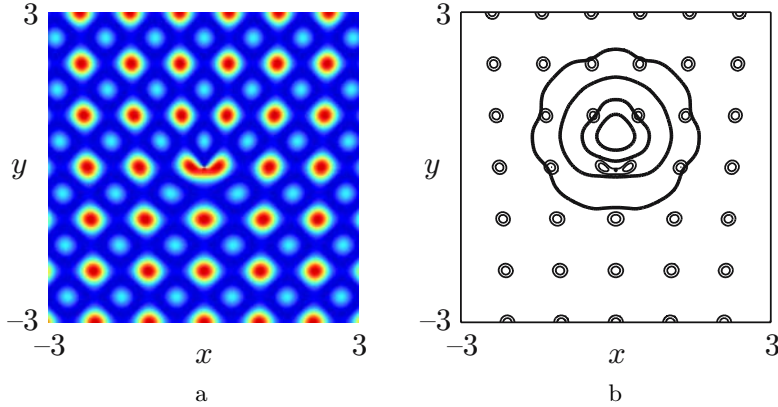


Fig. 2. Same as Fig. 1 for a lattice with an edge dislocation (Eq. (5)), using the same lattice parameters and $\mu = 0.5$ as in Fig. 1. The soliton’s peak is located at $(0, 0.68)$.

4. Edge dislocation

A lattice with an *edge dislocation*, analogous to those that can be found in atomic crystals [8], [12], can be similarly obtained from Eq. (3) with

$$V(x, y) = \frac{V_0}{25} \{2 \cos[k_x x + \theta(x, y)] + 2 \cos(k_y y) + 1\}^2, \quad (5)$$

where $k_x = k_y = K$ and the phase-dislocation function is $\theta(x, y) = 3\pi/2 - \arctan(y/x)$. It is clear from Fig. 2a that this dislocation is unlike a point defect because the density of lattice sites changes vertically across the lattice. Despite this strong irregularity, we find solitons in the vicinity of the phase dislocation. It is clear from Fig. 2b that the soliton is asymmetric. The soliton center is located above the phase dislocation between neighboring local maximums of the lattice. In this respect, it is like a soliton with a center near a lattice minimum. We note that the starting point of the computational method is near the origin and the solution moves upward along the y axis during the iterations until convergence is attained.

A striking observation in Fig. 7 below is that the gap edge with an edge dislocation occurs for $0.9 < \mu_{\max} < 0.95$, which is considerably smaller than for the other lattices. In fact, an interesting phenomenon occurs as μ increases during the computation. When $\mu = 0.9$, a reliable convergence is attained ($\delta = 10^{-10}$; see the appendix for the definition of δ), and the solution in this case is between the local maximums, as shown in Fig. 3a. When $\mu = 0.95$, the solution initially converges at the same location (with $\delta = 10^{-5}$). But this “convergence” is misleading because the solution moves upward along the y axis with further iterations, “sliding” up between two local maximums and eventually converging (with $\delta = 10^{-10}$) between the four local maximums that are one lattice cell above the edge dislocation (Fig. 3b). Further investigations reveal that for $0.95 < \mu < 2$, the solitons remain one lattice cell above the dislocation. These solitons “see” a more periodic lattice because the nearest four lattice maximums are approximately symmetric and equispaced, and the solitons are therefore more similar to periodic square-lattice solitons. In fact, the eigenvalue dependence of the soliton power is very similar to that of a periodic lattice (see Fig. 7). Thus, the edge dislocation clearly reduces the size of the effective nonlinear gap.

5. Penrose quasicrystal solitons

We next investigate solitons on *quasicrystal lattices*. Such lattices appear naturally in certain molecules [6], [8], and they have been generated and studied in optics [20]–[22] and also studied in BECs [23].

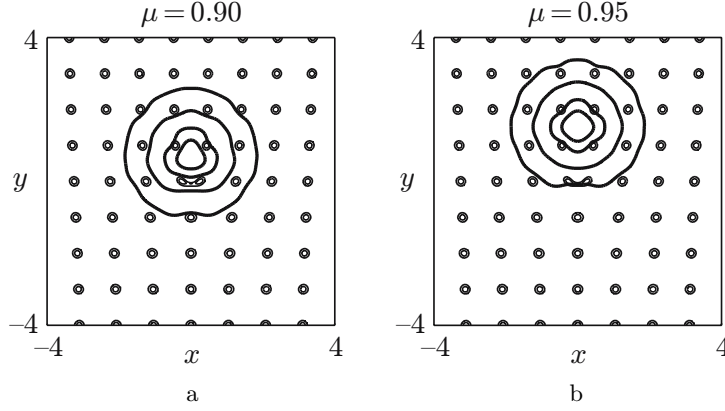


Fig. 3. When the propagation constant is $\mu \geq 0.95$, the soliton shifts one lattice cell upward along the y axis during the convergence process. The effective nonlinear gap edge with an edge dislocation occurs for $0.9 < \mu_{\max} < 0.95$.

Importantly, Freedman et al. recently predicted and observed solitons in Penrose quasicrystals generated using the optical-induction method [24]. In this study, the optical potential was formed by the far-field diffraction pattern of a mask with point apertures located at the N vertices of a regular polygon. The corresponding potential is given by

$$V_N(x, y) = \frac{V_0}{N^2} \left| \sum_{n=0}^{N-1} e^{i(k_x x + k_y y)} \right|^2, \quad (6)$$

where $(k_x, k_y) = (K \cos(2\pi n/N), K \sin(2\pi n/N))$. Potential (6) with $N = 2, 3, 4, 6$ yields periodic lattices corresponding to standard 2D crystal structures. All other values of N correspond to quasicrystals, which have a local symmetry near the origin and long-range order but, in contrast to periodic crystals, are not invariant under spatial translation [7]. Below, we focus on the case $N = 5$ (see Fig. 4a), whose lattice is often called a Penrose quasicrystal.

On the Penrose lattice, we find solitons centered near the origin, which is the global maximum of the lattice potential (see Fig. 4b). Similar to solitons centered at the maximums of periodic lattices, these Penrose solitons have a dimple at their center (see Fig. 5). Further investigations reveal that Penrose solitons centered around local minimums do not have a dimple, similar to their periodic-lattice counterparts (see Fig. 6).

We note that in some previous studies of Penrose lattices, different lattices were considered with cylinders of Kerr material located at the vertices of a (virtual) Penrose tile surrounded by air [20]–[22], [25], [26]. The medium we consider here is homogeneous and has a constant Kerr coefficient and continuous modulation of linear refractive index (6).

6. Power–eigenvalue relation

To compare the different lattice solitons centered near either local minimums or maximums, we plot the soliton power $P = \int f^2(x, y) dx dy$ in Fig. 7 as a function of the eigenvalue μ for all the lattices studied above and also for the corresponding periodic square lattice (i.e., Eq. (4) with $\theta(x, y) \equiv 0$). We note that all these lattices have the same peak depth $V_0 = 12.5$ and also background wave number $K = 2\pi$, where K can be considered a “local” wave number for the Penrose lattice (see Eq. (6)).

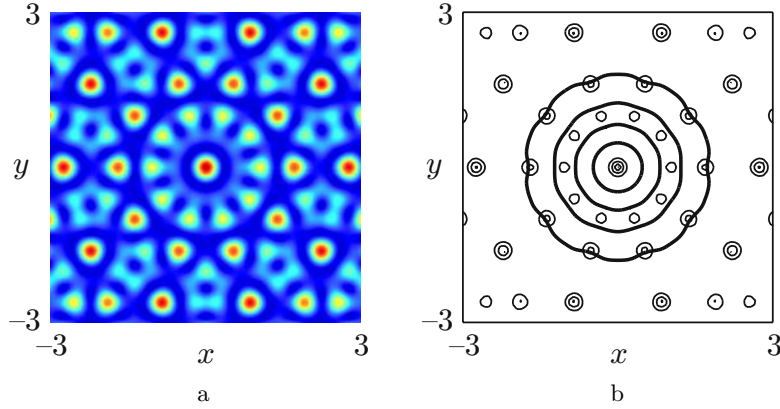


Fig. 4. Same as Fig. 1 for a Penrose lattice (Eq. (6) with $N = 5$) and the corresponding soliton centered at the center (maximum), using the same lattice parameters and $\mu = 0.5$ as in Fig. 1.

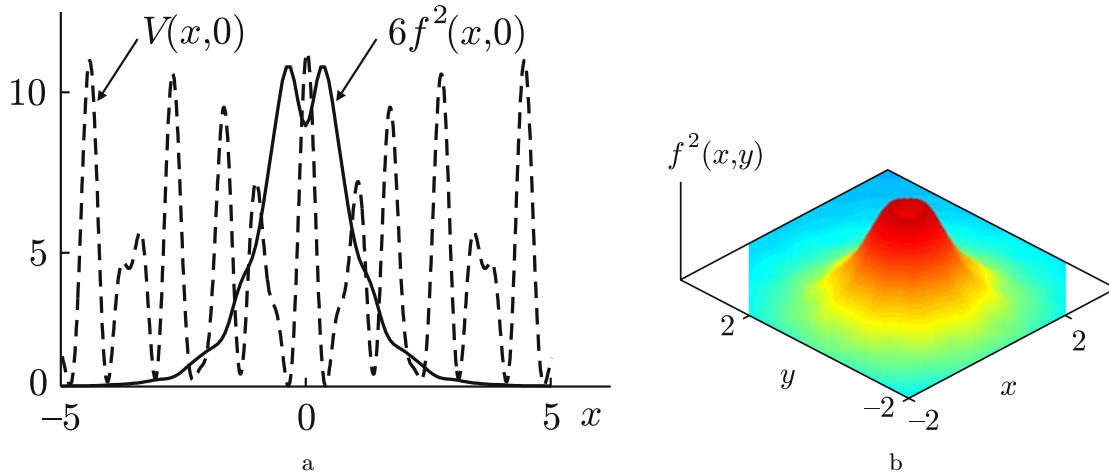


Fig. 5. Similar to solitons centered at the maximums of periodic lattices, Penrose solitons can have a dimple, which becomes more pronounced for large values of μ , i.e., near the gap edge. (a) Cross section along the y axis of a Penrose soliton ($6f^2(x,0)$, solid line) with $\mu = 2$, superimposed on the underlying lattice potential $V(x,0)$ (dashed line). (b) Soliton intensity in a 3D view showing the dimple.

Localized modes are calculated in the semi-infinite gap $\mu < \mu_{\max}$ for some lattice-dependent μ_{\max} . When the eigenvalue exceeds μ_{\max} , the numerical method typically converges to an extended state (but see below for exceptions). In addition, comparison reveals the following (see Fig. 7):

1. The power of vacancy-defect, edge-dislocation, and Penrose-quasicrystal lattice solitons is lower than their periodic counterparts for a considerable range of eigenvalues. In particular, of all the lattices studied here, the vacancy-defect and edge-dislocation solitons have the lowest power.
2. A vacancy defect has little effect on the gap size ($\mu_{\max} \approx 2$), but it significantly reduces the power threshold, i.e., the minimal soliton power throughout the gap. But it is noteworthy that the power threshold is positive for all these potentials.
3. An edge dislocation (dashed line) reduces the gap size ($0.9 < \mu_{\max} < 0.95$), as explained in Sec. 4.

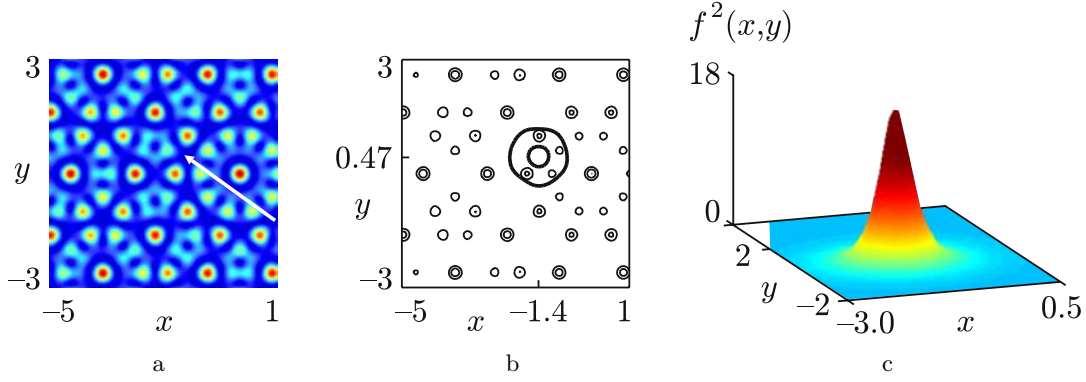


Fig. 6. (a) A soliton centered near a local minimum at the point $(-1.4, 0.47)$ (the arrow shows the point) of the Penrose lattice, using the same lattice parameters as in Fig. 4 and $\mu = -1$. (b) Contour plot of the soliton amplitude superimposed on the background lattice. (c) Soliton intensity in a 3D plot showing that the soliton profile decays monotonically (i.e., does not have a dimple).

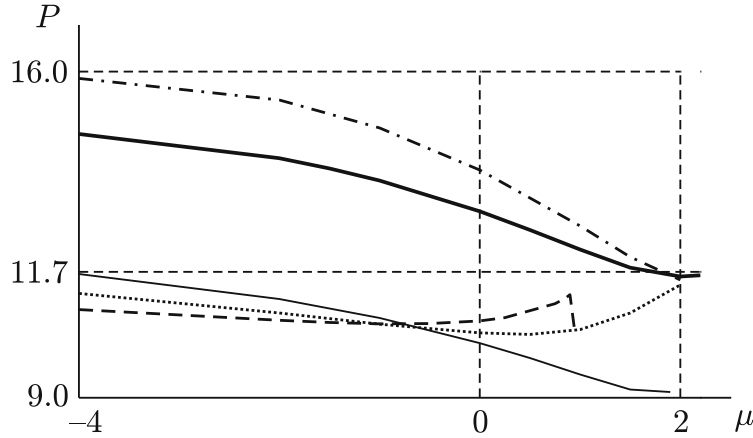


Fig. 7. Soliton power P as a function of the eigenvalue μ in the semi-infinite band-gap for the Penrose lattice (thick line), vacancy-defect lattice (thin line), and edge-dislocation lattice (dashed line). The powers of solitons centered at the maximum (dot-dashed line) and minimum (dotted line) of a periodic square lattice are also shown. All lattices have the same peak depth $V_0 = 12.5$ and background wave number $K = 2\pi$. We note that the solitons become narrower as μ decreases.

4. A Penrose soliton has a slightly larger gap size ($\mu_{\max} \approx 2.2$) compared with solitons on a periodic square lattice. But solitons centered near the maximums of periodic square and Penrose lattices have a similar power behavior, which is somewhat unexpected because these lattices have very different structures.

7. Evolution and stability

The question of soliton evolution under perturbations is important for applications. To study this, we directly compute Eq. (1) using the various potentials, where the initial conditions are the soliton with a 1% random noise in the amplitude and phase. In the general case, we find the following:

Solitons centered near lattice minimums oscillate with a small amplitude for $dP/d\mu < 0$ (see Fig. 8, which shows stability with a vacancy-defect lattice) and with a large amplitude for $dP/d\mu > 0$ (see

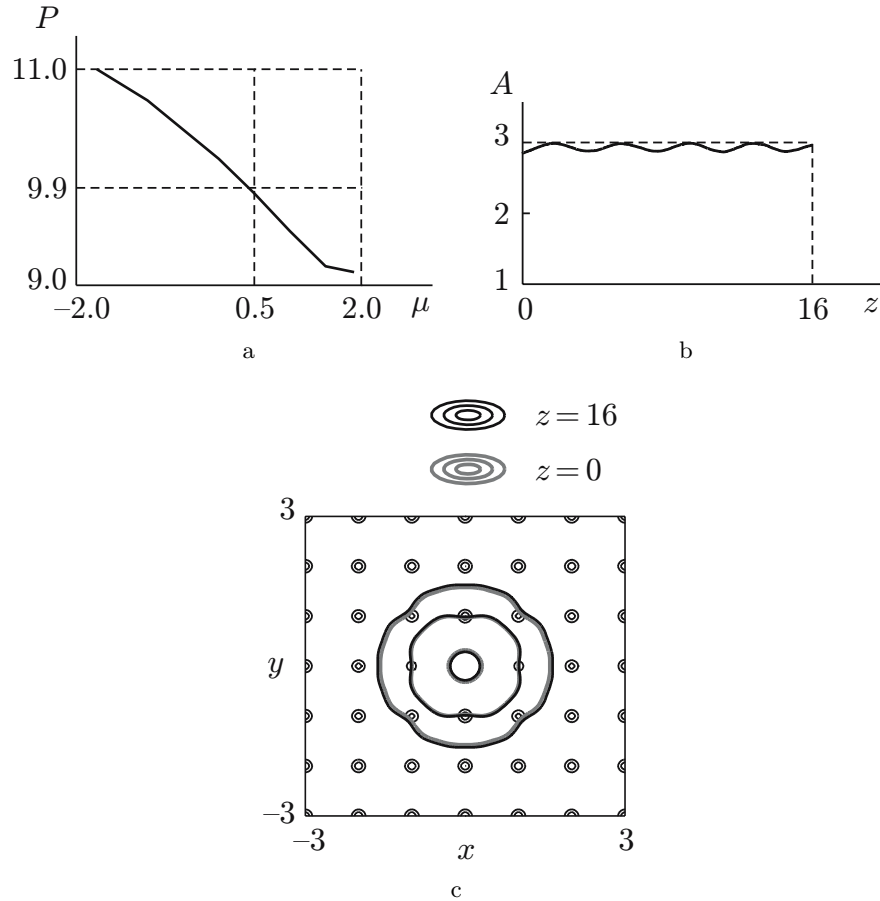


Fig. 8. Evolution of a soliton situated at the vacancy of the potential (Eq. (4) with $V_0 = 12.5$ and $K = 2\pi$ and Fig. 1) and $\mu = 0.5$. (a) The slope (i.e., $dP/d\mu$) is negative with these parameters. (b) Peak amplitude $A(z) = \max_{x,y} |u(x, y, z)|$ of the solution of Eq. (1) as a function of the propagation distance. The initial conditions are taken as the soliton with a 1% noise in the amplitude and phase. The soliton remains very stable during propagation. (c) Superimposed contour plots of the input soliton ($z = 0$) and the solution after a propagation of 16 diffraction lengths ($z = 16$), which are almost indistinguishable, on top of the underlying vacancy potential.

Fig. 9, which shows instability with an edge-dislocation lattice).

Solitons centered near lattice maximums typically collapse after a finite propagation distance (see Fig. 10 with a Penrose lattice).

8. High-order quasicrystal solitons

The Penrose lattice is a quasicrystal lattice of the fifth order, i.e., is described by Eq. (6) with $N = 5$. It is interesting to investigate quasicrystal lattice solitons of higher orders. We consider the case where the impinging waves are separated by N equal angles, i.e.,

$$V_N(x, y) = \frac{V_0}{N^2} \left| \sum_{n=0}^{N-1} e^{iK(x \cos \theta_n + y \sin \theta_n)} \right|^2, \quad (7)$$

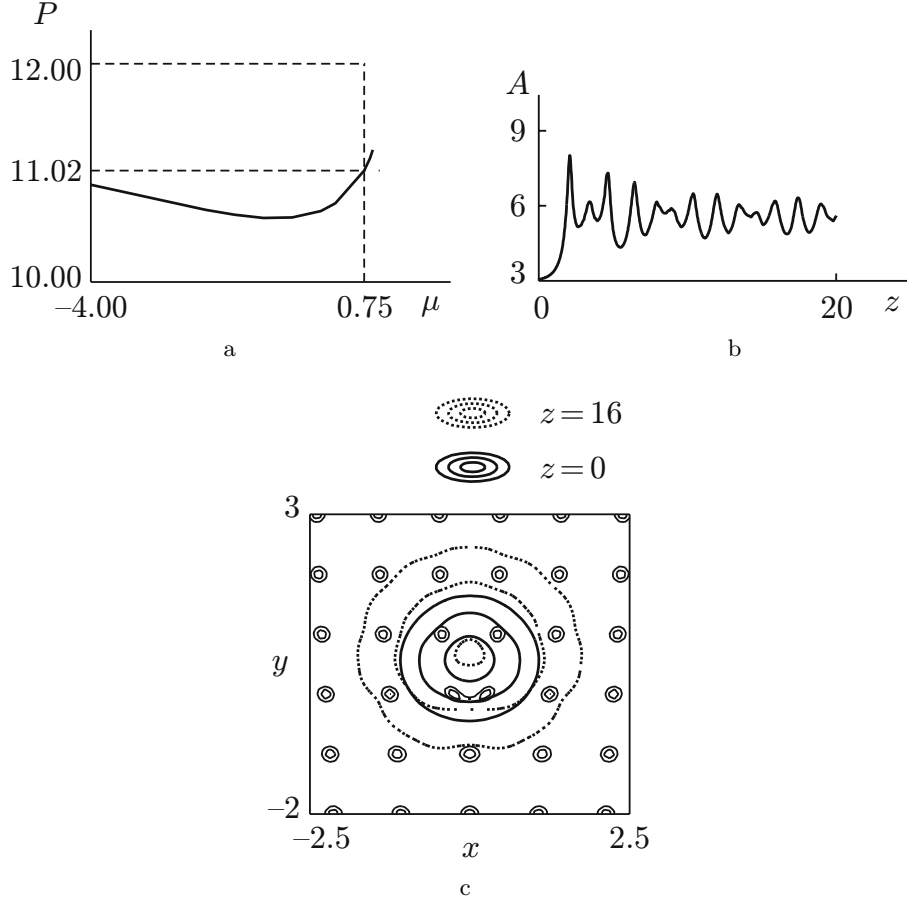


Fig. 9. Same as Fig. 8 for a soliton on an edge-dislocation lattice (Eq. (5) and Fig. 2) with $\mu = 0.75$. (a) The slope is positive with these parameters. (b) The solution undergoes large but bounded focusing-defocusing oscillations during propagation. (c) The solution considerably narrows down during propagation, i.e., the full width at half maximum of $|u(x, y, z)|^2$ decreases by approximately a half from the input at $z = 0$ (solid line) to the output at $z = 20$ (dotted line).

where $\theta_n = 2\pi n/N$. In the limit of an infinite number of waves $N \rightarrow \infty$, the quasicrystal lattice approaches the Bessel lattice. This can be established using Riemann sums with $\Delta\theta \equiv 2\pi/N$:

$$\begin{aligned} \lim_{N \rightarrow \infty} V_N(x, y) &= \frac{V_0}{(2\pi)^2} \lim_{\Delta\theta \rightarrow 0} \left| \sum_{n=0}^{2\pi/\Delta\theta - 1} e^{iK(x \cos \theta_n + y \sin \theta_n)} \frac{1}{\Delta\theta} \right|^2 = \\ &= \frac{V_0}{(2\pi)^2} \left| \int_0^{2\pi} e^{iK(x \cos \theta + y \sin \theta)} d\theta \right|^2 = V_0 J_0^2(Kr), \end{aligned}$$

where $r = \sqrt{x^2 + y^2}$ and $J_0(r)$ is the zeroth-order Bessel function, used in the integral representation [27]. As N increases, the angular distance between the lattice maximums (and minimums) decreases at any given radius, and the limiting Bessel lattice ($N = \infty$) has continuous rings of maximums (see Fig. 11). We note that Bessel solitons were recently investigated [28].

It can be seen from Fig. 12a that the tenth-order quasicrystal lattice ($N = 10$) differs significantly from the Penrose quasicrystal ($N = 5$). On the other hand, the tenth-order quasicrystal is very similar to the

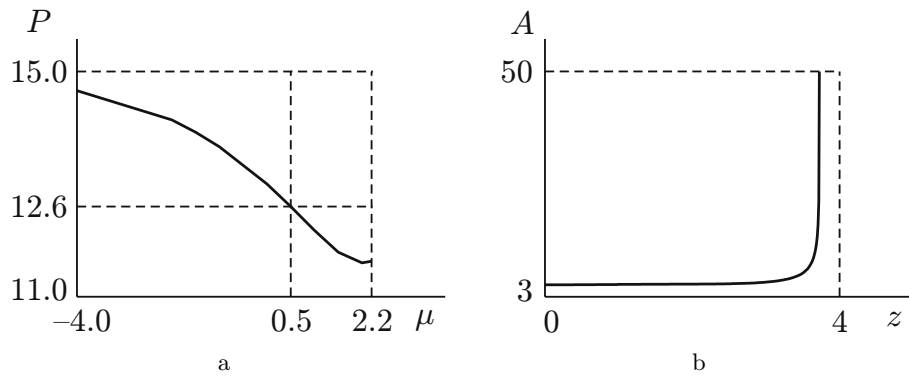


Fig. 10. Same as in Fig. 8a and 8b for a soliton on a Penrose lattice (Eq. (6) and Fig. 4) with $\mu = 0.5$. (a) The slope is negative with these parameters. (b) The solution collapses at $z \approx 3.7$, i.e., its peak amplitude blows up as its width decreases to zero.

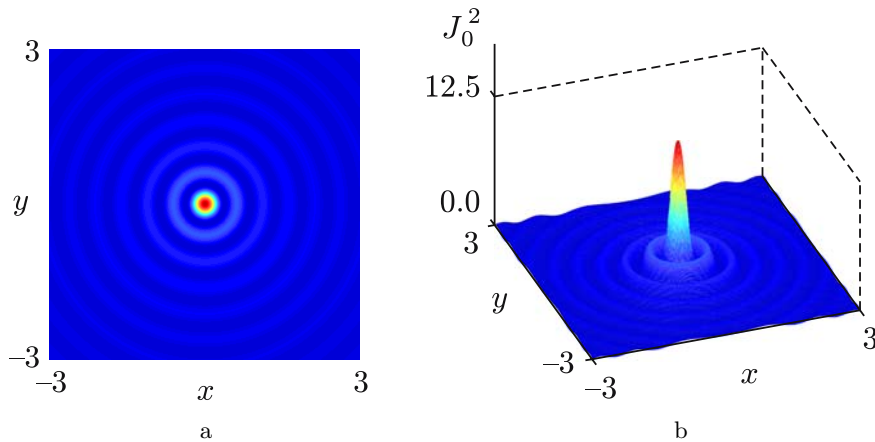


Fig. 11. (a) Contour and (b) 3D plots of a Bessel lattice.

Bessel lattice $N = \infty$ (or $J_0^2(r)$ in the figure). Therefore, the soliton profiles corresponding to a tenth-order quasicrystal and a Bessel lattice are approximately the same. This is particularly true for narrow solitons because the discrepancy between the lattices is in the wings and the solitons are almost identical near the origin. But the power–eigenvalue behavior changes significantly for wide solitons. More precisely, as N increases, the gap edge decreases as

$$\mu_{\max}[V_N] \xrightarrow{N \rightarrow \infty} +0,$$

while the power at the edge of the gap increases indefinitely (see Fig. 12b).

9. Conclusions

We have demonstrated the existence of stable 2D solitons in self-focusing media with irregular lattice potentials having vacancy defects, edge dislocations, and quasicrystal structures. Based on the results of computations, we can conclude that Penrose solitons are similar to solitons on periodic-lattice maximums while the vacancy-defect and edge-dislocation solitons differ significantly from their periodic-lattice counterparts.

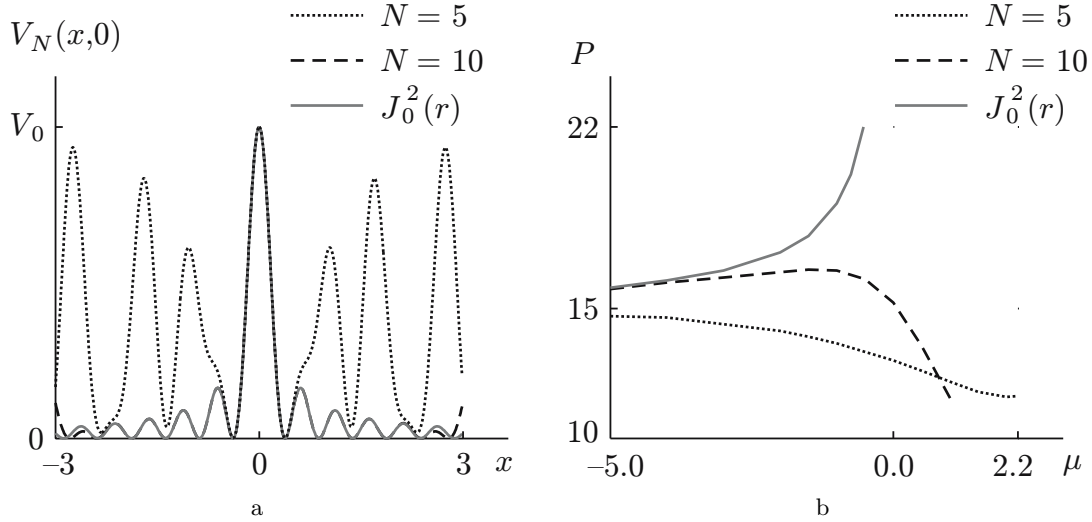


Fig. 12. (a) Cross sections $V_N(x,0)$ of the potentials $V_N(x,y)$ given by Eq. (7) with $V_0 = 12.5$ and $K = 2\pi$ for a Penrose quasicrystal ($N = 5$, dotted line), a tenth-order quasicrystal ($N = 10$, dashed line, barely distinguishable from the solid line), and a Bessel lattice ($N = \infty$, solid line). (b) Power versus eigenvalue for solitons on the three lattices in (a).

Appendix: Numerical method for computing solitons

To solve Eq. (2), we use a fixed-point spectral computational method [18], as explained below. Applying the Fourier transformation to Eq. (2) and adding and subtracting a term $r\hat{u}$, where $r > 0$ is a constant, we obtain

$$\hat{f}(\nu) = \widehat{R}[\hat{f}] \equiv \frac{(r + \mu)\hat{f} + \mathcal{F}\{|f|^2 - V(x,y)\}f}{r + |\nu|^2},$$

where $\nu = (\nu_x, \nu_y)$ are the Fourier variables, \mathcal{F} denotes the Fourier transformation, and the constant r is needed to avoid a singularity in the denominator (we use $r = 5$). We introduce a new field variable $f(x,y) = \lambda w(x,y)$, where $\lambda \neq 0$ is a constant to be determined. The iteration method takes the form $\widehat{w}_{m+1} = \lambda_m^{-1} \widehat{R}[\lambda_m \widehat{w}_m]$, $m = 0, 1, 2, \dots$, where λ_m satisfies the associated *algebraic condition*

$$\iint_{-\infty}^{+\infty} |\widehat{w}_m(\nu)|^2 d\nu = \lambda_m^{-1} \iint_{-\infty}^{+\infty} \widehat{R}[\lambda_m \widehat{w}_m] \widehat{w}_m^*(\nu) d\nu.$$

It has been found that this method prevents the numerical scheme from diverging. Thus, the soliton is obtained from a convergent iterative scheme (also see [29] for an alternative procedure in the case where there is a well-defined homogeneity). The initial point $w_0(x,y)$ is typically chosen to be Gaussian. The iterations stop when the relative error $\delta = |\lambda_{m+1}/\lambda_m - 1|$ reaches 10^{-10} . We note that convergence is attained quickly but slows as the mode becomes more extended, i.e., as μ approaches the (nonlinear) gap edge. We also note that the convergence of a similar method was proved under suitable assumptions on the potential [30].

Acknowledgments. This work was supported in part by the Office of Scientific Research of the United States Air Force (Grant No. FA9550-06-1-0237) and the National Science Foundation (Grant No. DMS0505352).

REFERENCES

1. D. N. Christodoulides, F. Lederer, and Y. Silberberg, *Nature*, **424**, 817 (2003).
2. A. A. Sukhorukov, Y. S. Kivshar, H. S. Eisenberg, and Y. Silberberg, *IEEE J. Quant. Electronics*, **39**, 31 (2003).
3. N. K. Efremidis et al., *Phys. Rev. Lett.*, **91**, 213906 (2003).
4. J. W. Fleischer, M. Segev, N. K. Efremidis, and D. N. Christodoulides, *Nature*, **422**, 147 (2003).
5. D. Neshev, Y. S. Kivshar, H. Martin, and Z. Chen, *Opt. Lett.*, **29**, 486 (2004).
6. D. Shechtman, I. Blech, D. Gratias, and J. W. Cahn, *Phys. Rev. Lett.*, **53**, 1951 (1984).
7. M. Senechal, *Quasicrystals and Geometry*, Cambridge Univ. Press, Cambridge (1995).
8. M. P. Marder, *Condensed Matter Physics*, Wiley, New York (2000).
9. F. Fedele, J. Yang, and Z. Chen, *Stud. Appl. Math.*, **115**, 279 (2005).
10. H. Buljan et al., *Stud. Appl. Math.*, **115**, 173 (2005).
11. L. Guidoni, C. Triché, P. Verkerk, and G. Grynberg, *Phys. Rev. Lett.*, **79**, 3363 (1997).
12. E. Schonbrun and R. Piestun, *Opt. Eng.*, **45**, 028001 (2006).
13. T. Pertsch et al., *Opt. Lett.*, **29**, 468 (2004).
14. M. Qi et al., *Nature*, **429**, 538 (2004).
15. W. Cai and R. Piestun, *Appl. Phys. Lett.*, **88**, 111112 (2006).
16. C. J. Pethick and H. Smith, *Bose–Einstein Condensation in Dilute Gases*, Cambridge Univ. Press, Cambridge (2001).
17. J. F. Nye and M. V. Berry, *Proc. Roy. Soc. London A*, **336**, 165 (1974).
18. M. J. Ablowitz and Z. H. Musslimani, *Opt. Lett.*, **30**, 2140 (2005).
19. M. S. P. Eastham, *The Spectral Theory of Periodic Differential Equations*, Scottish Academy Press, Edinburgh (1973).
20. R. T. Bratfalean et al., *Opt. Lett.*, **30**, 424 (2005).
21. R. Lifshitz, A. Arie, and A. Bahabad, *Phys. Rev. Lett.*, **95**, 133901 (2005).
22. W. Man, M. Megens, P. J. Steinhardt, and P. M. Chaikin, *Nature*, **436**, 993 (2005).
23. L. Sanchez-Palencia and L. Santos, *Phys. Rev. A*, **72**, 053607 (2005).
24. B. Freedman et al., *Nature*, **440**, 1166 (2006).
25. P. Xie, Z.-Q. Zhang, and X. Zhang, *Phys. Rev. E*, **67**, 026607 (2003).
26. A. Della Villa et al., *Phys. Rev. Lett.*, **94**, 183903 (2005).
27. M. Abramowitz and I. A. Stegun, eds., *Handbook of Mathematical Functions with Formulas, Graphs, and Mathematical Tables*, Dover, New York (1966).
28. Y. V. Kartashov, V. A. Vysloukh, and L. Torner, *Phys. Rev. Lett.*, **93**, 093904 (2004).
29. Z. H. Musslimani and J. Yang, *J. Opt. Soc. Amer. B*, **21**, 973 (2004).
30. D. E. Pelinovsky, A. A. Sukhorukov, and Y. S. Kivshar, *Phys. Rev. E*, **70**, 036618 (2004).